Microstructure and mechanical properties of pure Cu processed by high-pressure torsion

Edalati, Kaveh
Department of Materials Science and Engineering, Faculty of Engineering, Kyushu University

Fujioka, Tadayoshi
Department of Materials Science and Engineering, Faculty of Engineering, Kyushu University

Horita, Zenji
Department of Materials Science and Engineering, Faculty of Engineering, Kyushu University

https://hdl.handle.net/2324/26373

KYUSHU UNIVERSITY

Microstructure and mechanical properties of pure Cu processed by high-pressure torsion

Kaveh Edalati, Tadayoshi Fujioka, Zenji Horita*

Department of Materials Science and Engineering, Faculty of Engineering, Kyushu University, Fukuoka 819-0395, Japan

Abstract

Pure Cu was subjected to severe plastic deformation through high-pressure torsion (HPT) using disc and ring samples. Vickers microhardnesswas measured across the diameter and itwas shownthat all hardness values fall well on a unique single curve regardless of the types of the HPT samples when they are plotted against the equivalent strain. The hardness increases with an increase in the equivalent strain at an early stage of straining but levels off and enters into a steady-state where the hardness remains unchanged with further straining. It was confirmed that the tensile strength also follows the same single function of the equivalent strain as the hardness. The elongation to failure as well as the uniform elongation also exhibits a single unique function of the equivalent strain. Transmission electron microscopy showed that a subgrain structure develops at an early stage of straining with individual grains containing dislocations. The subgrain size decreases while the misorientation angle increases and more dislocations are formed within the grains with further straining. In the steady-state range, some grains appear which are free from dislocations, suggesting that recrystallization occurs during or after the HPT process. The mechanism for the grain refinement was discussed in terms of dislocation mobility.

Keywords: Severe plastic deformation; High-pressure torsion; Copper; Equivalent strain; Stacking fault energy

*Corresponding author. Tel.: +81 92 802 2992; fax: +81 92 802 2992.
  E-mail address: horita@zaiko.kyushu-u.ac.jp (Z. Horita).

1. Introduction

Considerable interest has developed over the last decade in processing materials through the application of severe plastic deformation (SPD) in order to achieve grain sizes at the submicrometer or nanometer level [1–3]. Although several different SPD processing techniques are available, the most promising procedure appears to be the high-pressure torsion (HPT) [4,5]. Experiments have shown that HPT is especially effective in producing extremely small grain sizes when compared with other SPD processing techniques [6–8].

Bridgman who proposed the idea of HPT suggested the use of a cylindrical hollow specimen to produce a homogeneous

microstructure [9]. This idea was further developed by Erbel [10] and Saunders and Nutting [11], and very recently by Harai et al. who carried out HPT using ring samples with a simple modification of the technology currently in use for disc samples [12].

The strain in HPT is introduced in proportion to the distance from the disc center so that the strain at the disc center is theoretically zero and accordingly the microstructural development is inhomogeneous across the disc diameter [13–18]. However, the use of ring samples overcomes such a microstructural inhomogeniety and homogeneous microstructure is developed throughout the sample. The advantage of using the ring sample is that not only a homogeneous microstructure is developed but also the diameter of the ring can be increased by the area corresponding to the central hollow area [12].

Using both disc and ring samples, Harai et al. [12] showed that the hardness variation is represented as a unique function of the equivalent strain. High purity Al with 99.99% was used for this demonstration. The hardness initially increased to a maximum at an equivalent strain of ~2 and decreased with a further increase in the equivalent strain. The hardness leveled off at an equivalent strain of ~6 and this was followed by the onset of a steady-state where the hardness remained unchanged with straining. Along with this change in hardness, the microstructural evolution was examined in terms of dislocations and grain boundaries including misorientation angles using transmission electron microscopy and electron back scatter diffraction analysis [19,20].

In the present investigation, HPT using both disc and ring samples is applied to high purity Cu (99.99%) and the hardness variation with respect to equivalent strain is examined if it is expressed with a single unique function of the equivalent strain. The microstructural evolution is also examined with respect to the equivalent strain and the mechanism for grain refinement is discussed in comparison with pure Al.

2. Experimental materials and procedures

High purity copper (99.99%) was received in the form of a coldrolled plate having dimensions of 10mm×100mm×200mm. The plate was cut to cylinders with 10mm diameter and 10mm height and to inner-hollow cylinders with inner and outer diameters of 24 and 30mm using a wire-cutting electric discharge machine. Both cylinders were annealed for 1 h at 873K to give an initial grain size of ~150 μm. They were further sliced to discs and rings with thicknesses of 0.8mm.

HPT was conducted using the facilities as schematically illustrated in Fig. 1 for disc (left) and

ring (right) samples. The facilities consist of upper and lower anvils having a shallow hole of 10mm diameter and 0.25mm depth at the center for the disc sample. For the ring sample, the upper and lower anvils have a shallow circular groove with the inner and outer diameters of 24 and 30mm with the groove depth of 0.25mm around the center. Each sample was placed on the hole or on the groove and the upper and lower anvils were rotated with respect to each other at room temperature with a rotation speed of 0.5rpm under a selected pressure of 2 GPa. The rotation was terminated after a revolution of either 1/8, 1/4, 1, 2, 4 or 10. Fig. 2 shows the appearance of disc and ring samples after HPT for one revolution under a pressure of 2 GPa.
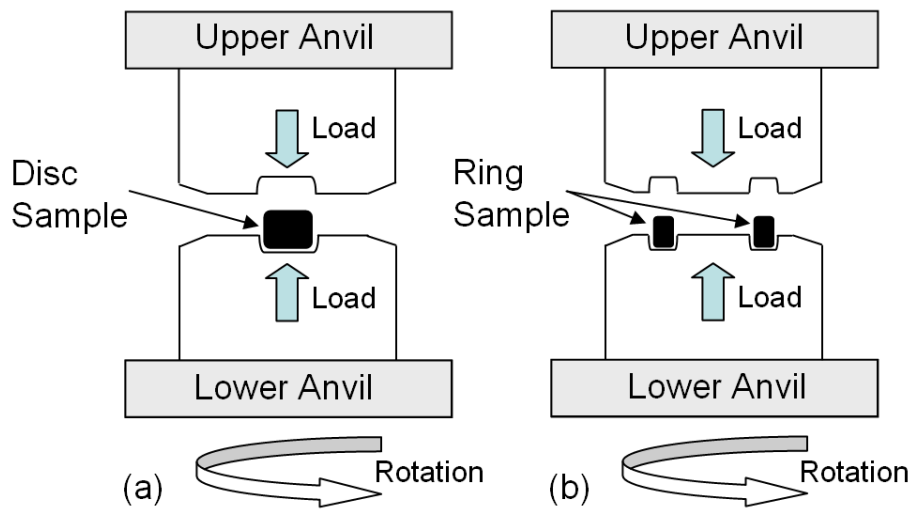

Fig. 1. Schematic illustration of HPT facilities for (a) disc and (b) ring samples.

Fig. 2. Appearance of disc (left) and ring (right) samples after HPT for one revolution.

The disc and ring samples subjected to HPT were evaluated in terms of Vickers hardness, tensile properties and microstructures. First of all, both ring and disc samples were polished to a mirror-like surface and the Vickers microhardness was measured along the radii from the center to edge at eight different radial directions with 0.5mmincrements as drawn by dotted lines in Fig. 3.

For each hardness measurement, a load of 200 g was applied for 15 s using an Akashi MVK-E3 testing machine. Second, the disc and ring samples were ground and polished to reduce the total thickness to 0.4mm. Thereafter, as illustrated in Fig. 3, miniature tensile specimens having 1mm gauge length and 1mm width were cut from both types of the samples using the wire-cutting electric discharge machining. Each tensile specimen was mounted horizontally on grips and pulled to failure using a tensile testing machine with an initial strain rate of 3.3×10^{-3} s^{-1}. The stress–strain curve was delineated for each specimen and the ultimate tensile strength and elongation to failure were measured from the curves. To obtain the average, at least three tensile tests were repeated on the samples processed at the same HPT conditions. Third, discs with 3mm in diameter were punched from the HPT discs at 2mmaway from the center and from the center of the ring width as also illustrated in Fig. 3. The 3mm discs were ground mechanically to a thickness of 0.15mm and further thinned for transmission electron microscopy (TEM) with a twin-jet electro-chemical polisher using a solution of 15% HNO_3, 15% $C_3H_5(OH)_3$ and 70% CH_3OH at 243K under an initial applied voltage of 20V and a subsequent voltage of 8.5 V. A Hitachi H-8100 transmission electron microscope was operated at 200 kV for the observation of microstructures. Selected area electron diffraction (SAED) patterns were taken from a region with 6.3μm diameter to complement the TEM observations.
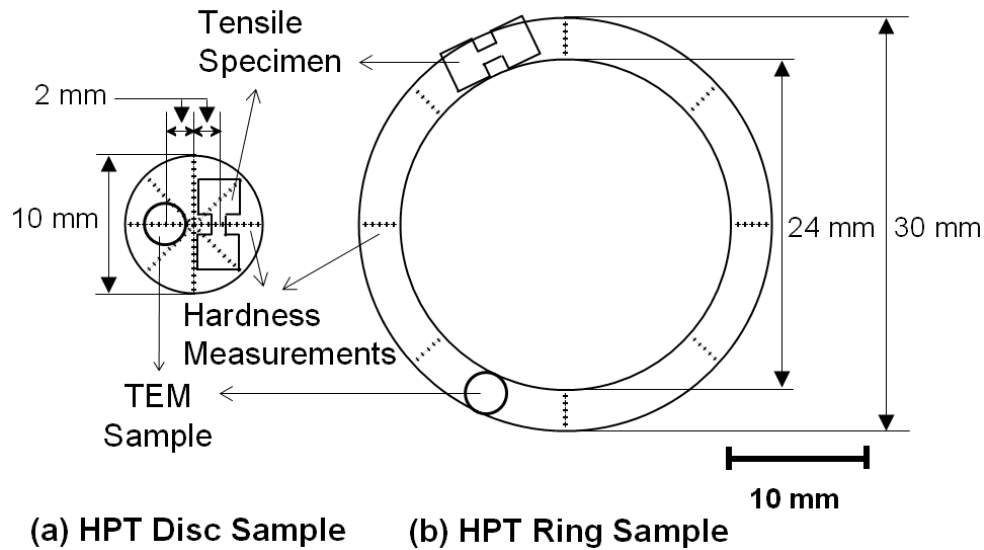

Fig. 3. Dimensions of (a) disc and (b) ring samples including positions for microhardness measurements and locations for TEM discs and tensile specimens.

3. Results

Fig. 4 shows the hardness variation with the distance from the centers of disc and ring samples after revolutions from 1/8 to 10 under a pressure of 2 GPa. The microhardness increases with an increasing number of revolutions and an increasing distance from the center for the disc samples. The saturation of the hardness level appears in the disc samples after one or more revolutions and in particular the hardness values after 10 revolutions lie close to this saturated level. The hardness is

almost constant within the width of the ring samples but there is a slight increase in the hardness level with an increasing number of the revolution.

As attempted in earlier paper [12], all hardness values in Fig. 4 are plotted against the equivalent strain in Fig. 5. Here, the equivalent strain was calculated as:

$$\varepsilon = \frac{r\theta/t}{\sqrt{3}} \qquad (1)$$

where r is the distance from the center of disc or ring, θ is the rotation angle in radian and t is the thickness of disc or ring. It is apparent that all points fall well on a single curve for both disc and ring samples and there is no difference in the hardness behavior between the disc and ring samples. The hardness increases with an increase in the equivalent strain at an early stage of straining but levels off and enters into a steady-state where the hardness remains unchanged with further straining.
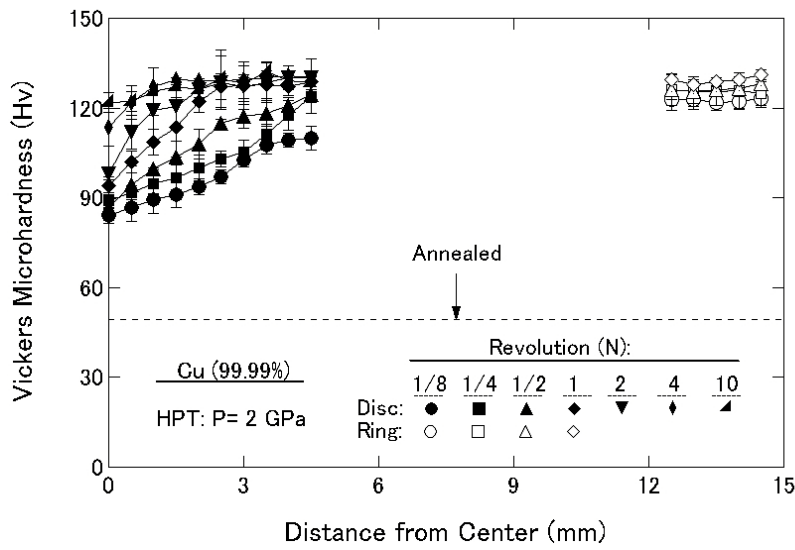

Fig. 4. Vickers microhardness plotted against distance from center for disc and ring samples processed after various revolutions.
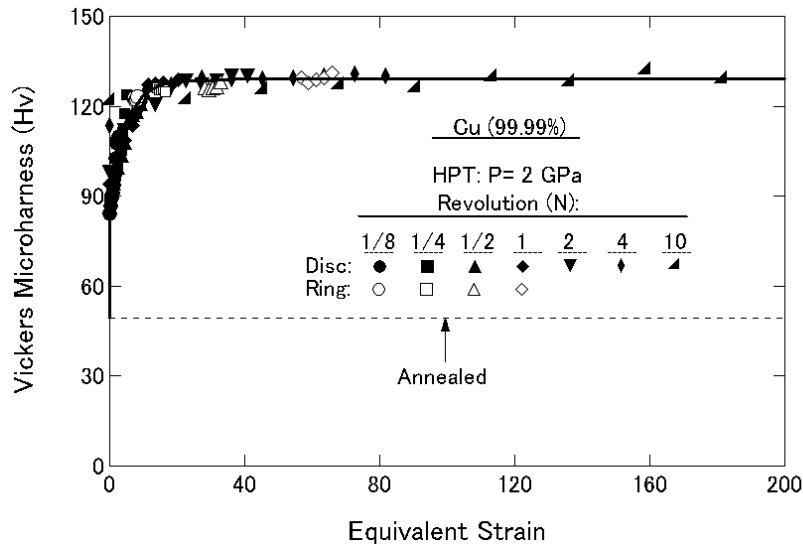

Fig. 5. Vickers microhardness plotted against equivalent strain for disc and ring samples processed after various revolutions (all data points shown in Fig. 4).

Fig. 6 plots the hardness variation along the periphery at the mid width of ring samples for revolutions of 1/8 to 1. Although most of the hardness values lie on a constant level, close examination reveals that the angular variation is smaller as the number of the revolution increases. This suggests that the local inhomogeneity is developed when the number of the revolution is small but as it is increased, the homogeneity is established through the ring sample.
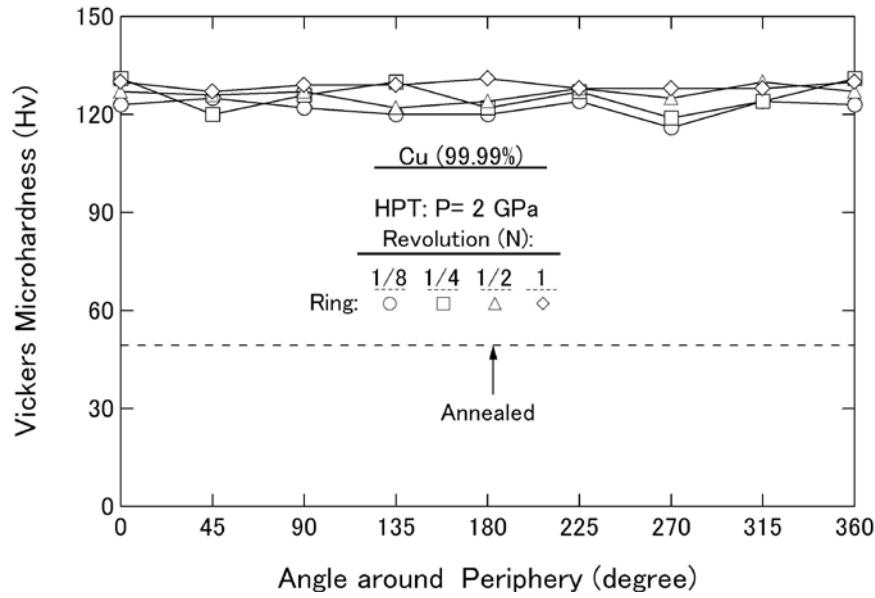

Fig. 6. Vickers microhardness plotted along periphery of ring samples at 13.5mm from center of ring samples processed after various revolutions.
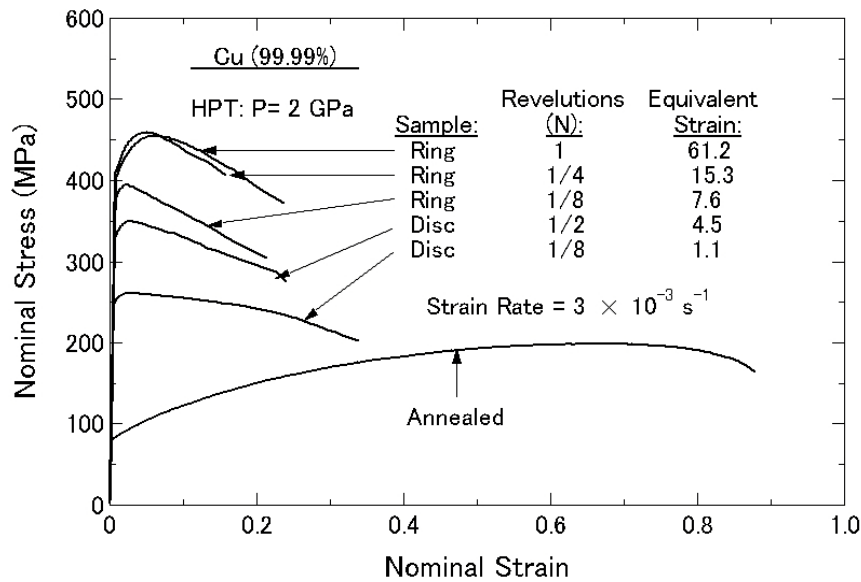

Fig. 7. Nominal stress versus nominal strain curves for annealed sample

The stress–strain curves are shown in Fig. 7 from tensile testing conducted at room temperature at an initial strain rate of 3.3×10^{-3} s^{-1} for both disc and ring samples. The tensile strength is increased but the total elongation to failure is decreased with an increase in the equivalent strain imposed by the HPT process. However, close inspection reveals that, while

6

maintaining higher strengths, there is some enhancement in the uniform strain which is defined as the strain at the maximum stress. In other words, the strain range for the work hardening region is very limited when the imposed strain is small but it gradually increases with an increase in the equivalent strain. It is noted that the tensile behavior should be different when compared with the standard size of the tensile specimens because the gauge length is the same size as the gauge width and thus the uniaxial tensile condition may not be achieved in the present miniature tensile specimen.

Tensile testing results are more clearly shown in Fig. 8(a)–(c) where the ultimate tensile strength is plotted against the equivalent strain and the elongation to failure and the uniform elongation are plotted against the equivalent strain, respectively. Fig. 8(a) shows that the tensile strength increases with increasing the equivalent strain, levels off at an equivalent strain of ~15 and remains constant with a further increase in the equivalent strain. This trend is very similar to the hardness variation with respect to the equivalent strain as plotted in Fig. 5. In fact, all values of the tensile strength fall well on the single curve determined by the hardness measurement when the tensile strength (σ) is converted to the hardness (Hv) through the relation as $\sigma = 3.4$Hv. Here, the value of 3.4 is well consistent with the factor, 3, accepted for the conversion. The variation of the ductility is shown in Fig. 8(b) where the total elongation to failure decreases with an increase in the equivalent strain and it appears to take a minimum at an equivalent strain of ~15 followed by a slight increase with a further straining. The uniform elongation is about 4% up to an equivalent strain of ~15 but there is an appreciable increase beyond the equivalent strain of ~15. It should be noted that the equivalent strain of ~15 for the onset of the steady-state is coincident with the strain where the ductility enhancement appears. As will be shown below, this may be attributed to the formation of recrystallized grains which are free from dislocations.

TEM micrographs and SAED patterns are shown in Fig. 9 from three samples subjected to different magnitudes of the equivalent strain: (a) ε = 1.1 after processing a 10-mm disk sample for 1/8 revolutions, (b) ε = 7.6 after processing a 30-mm ring sample for 1/8 revolutions, and (c)–(e) ε = 61.2 after processing a 30-mm ring for one revolution. The three samples correspond to an initial stage and a mid stage of the hardness increase and to a stage of the steady state, respectively. It is apparent from Fig. 9(a) at ε = 1.1 that the microstructure consists of subgrains with the average size of ~1 μm and there are some dislocations within them. Areas of high dislocation density are also locally visible within the subgrains as marked A. Because of a net type of the SAED pattern, the boundary misorientation should be very low. In Fig. 9(b) at ε = 7.6, the subgrains become smaller to the size of ~0.3 nm having many dislocations within them and the grain boundaries increased the misorientation angles because the diffractions spots are now diffused around rings. In Fig. 9(c) at ε = 61.2, the grains even become smaller to ~0.2 nm and the grain boundaries appear to be more straight and better defined. This is well demonstrated by the dark field image in Fig. 9(d) and a higher magnification image in Fig. 9(e). Note that the dark field image was taken with the diffracted beam indicated by an arrow in the SAED pattern. The ring pattern from the SAED analysis indicates that the small grains are separated by high angles of misorientations. Inspection of the high magnification view in Fig. 9(e) reveals that there are grains with a low density of dislocations

7

as marked B while some grains contain many dislocations. This suggests that recrystallization may have taken place during or after HPT processing.
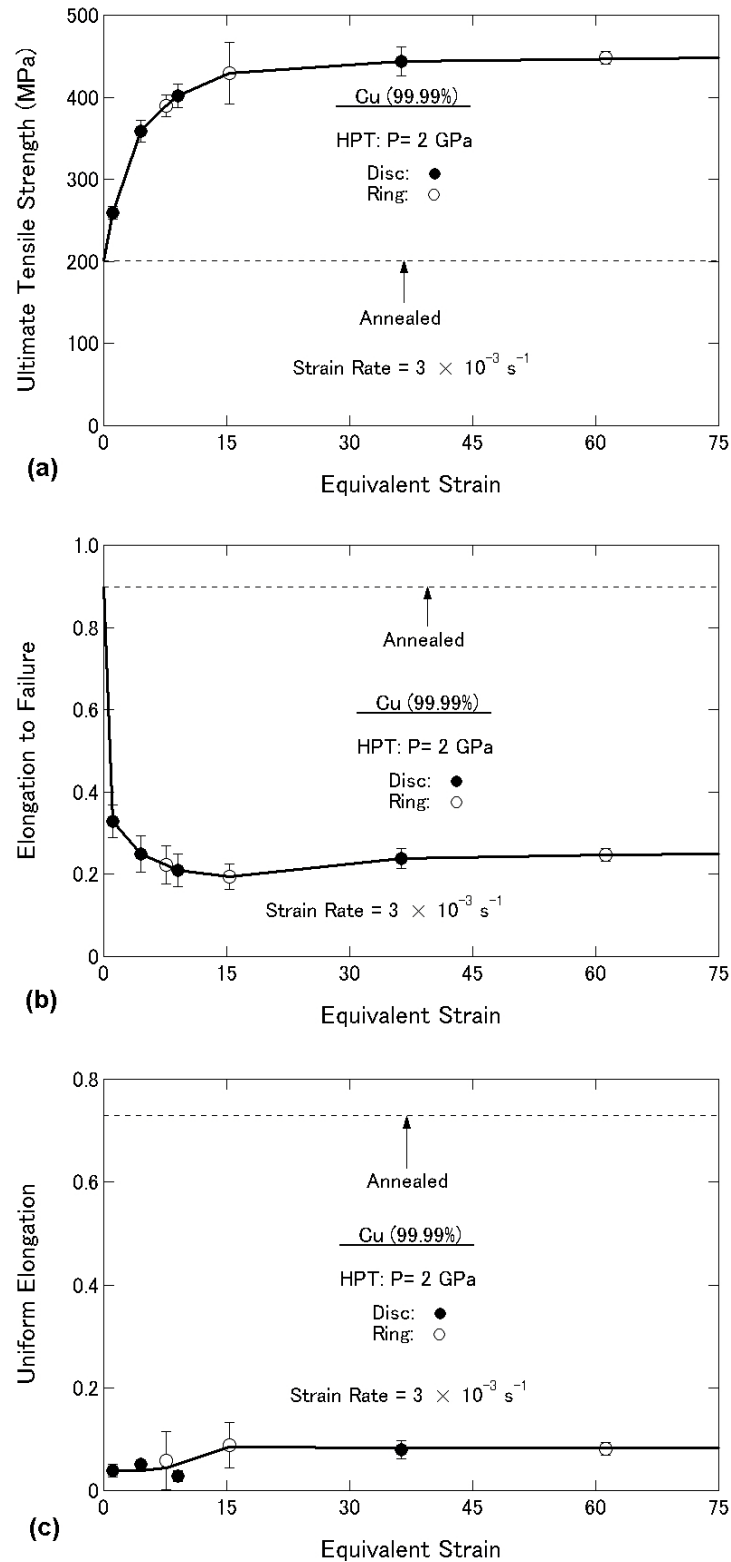

Fig. 8. Variation of (a) ultimate tensile strength, (b) elongation to failure and (c) uniform elongation with equivalent strain for some selected disc and ring samples.
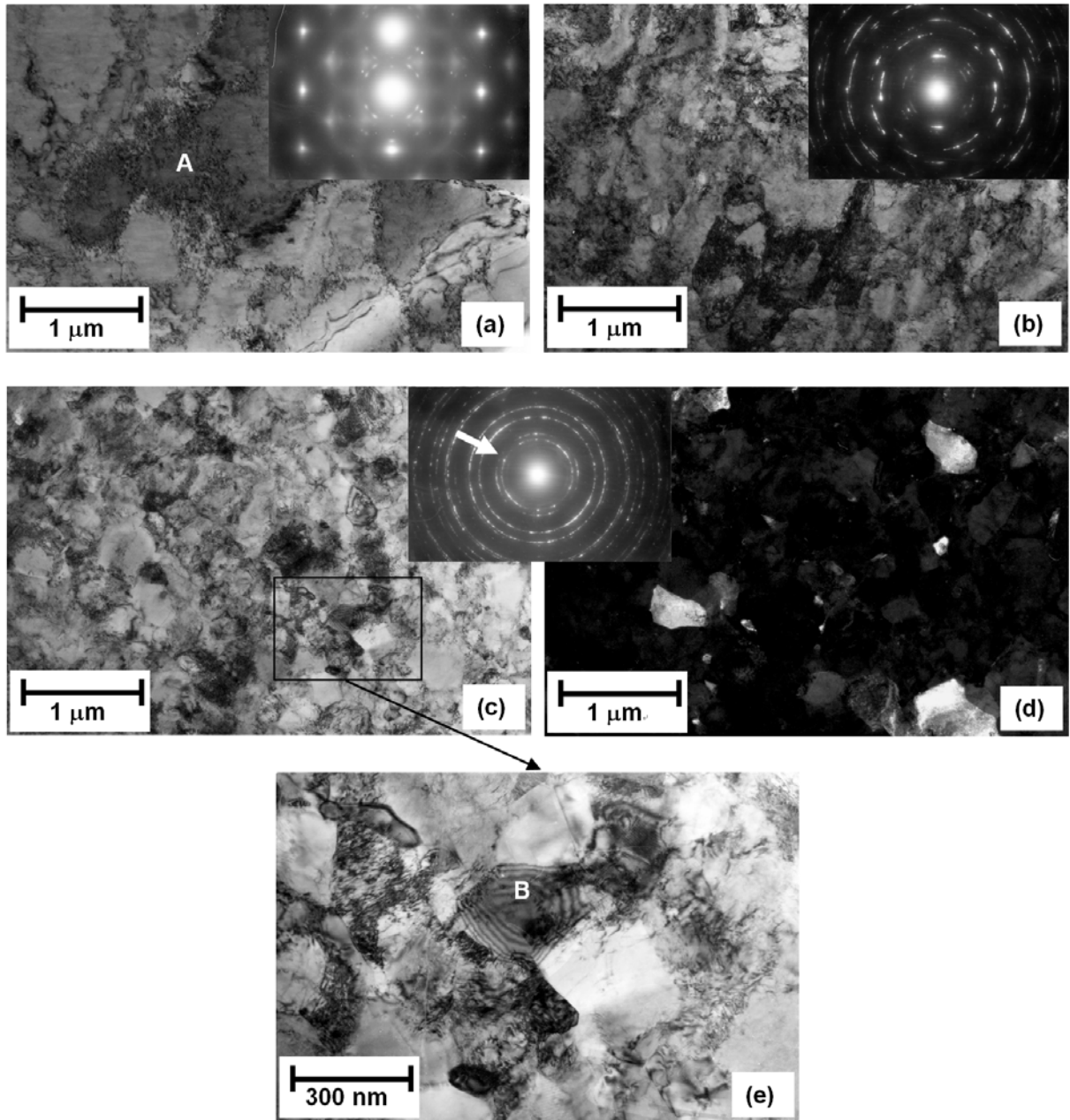
Fig. 9. TEM micrographs and SAED patterns for (a) disc sample after 1/8 revolutions, (b) ring sample after 1/8 revolution and (c) to (e) ring sample after 1 revolution, where (e) is magnified view of (c) and (d) is dark field image of (c).

4. Discussion

This study has shown that the hardness variation is expressed by a unique function of the equivalent strain so that all data points fall well on a single curve. This is also valid for the tensile strength and elongation to failure including uniform elongation. The present results thus indicate clearly that there is no difference between the disc samples and the ring samples for introducing strain despite the fact the higher strain rate is achieved in the ring sample because the diameter is larger than the disc sample. A comparison with the plot for pure Al with the purity level of 99.99% [12,19] reveals two important differences: (1) there is no hardness maximum in pure Cu but a clear

maximum in pure Al at equivalent strain of ~2 and (2) the steady-state, where the hardness remains constant with the equivalent strain, begins at equivalent strain of ~15 for pure Cu but at equivalent strain of ~6 for pure Al. These differences may be attributed to the dislocation mobility in the two metals. The dislocation mobility should be affected by three factors: (1) the presence of impurity elements, (2) the difference in stacking fault energy (SFE) and (3) the difference in the homologous temperature.

The first factor for the presence of impurity elements may be neglected in this study because both Al and Cu used in this study have the same purity level as 99.99%. Considering the second factor, it is well documented that there is a large difference in SFE between Al and Cu: 166 J/m^2 for Al but 36 J/m^2 for Cu [20]. This difference leads to the difference in the distance between the two dissociated partial dislocations: the former distance for Al is smaller and the latter Cu is larger so that dislocations are much easier to move in the crystal of Al than of Cu. It is reasonable to conclude that the difference in SFE has a large influence on the hardness behavior with respect to the equivalent strain.

Concerning the third factor, the melting points of Al and Cu are 933 and 1356 K, respectively, and therefore the room temperature (298K) corresponds to 0.32 and 0.22 when normalized by each of the melting points. This difference in the homologous temperature gives rise to the difference in diffusion distance such that it is 2.1×10^{-3} nm for Al and is 5.1×10^{-10} nm for Cu within 1 h. Considering 2/3 to 1/2 of the activation energy for the grain boundary diffusion or dislocation core diffusion [21,22], an estimation results in 10–730 nm for Al and 4.5×10^{-4} to 0.42nm for Cu. Although the diffusion distance in Cu is well below or comparable at most to the corresponding lattice constant, the distance in Al is in the order of the distance between two neighboring dislocations or of the grain size so that dislocations can annihilate each other through dislocation core diffusion or grain boundary diffusion.

It is therefore concluded that the advent of a maximum in pure Al is due to high mobility of dislocations so that dislocations annihilate each other through diffusion along dislocation cores and/or grain boundaries but the maximum does not appear because the diffusion is too low to cause any annihilation in Cu.

Fig. 10 schematically illustrates a variation in hardness with straining based on the measurement shown in Fig. 5 and a change in microstructure as observed in Fig. 9. Unlike the three stages in Al reported earlier [19], the hardness variation may be divided into two regions. In the first region (I), dislocations accumulate to form subgrains with an increasing population within individual grains. With further straining, the subgrain size decreases, the subgrain boundary width becomes better defined and the misorientation angle increases. In this change in the microstructure, the hardness levels off and reaches saturation. No change in hardness occurs with further straining and a steady-state is entered because a balance now holds between the hardness increase due to accumulation of dislocations and the decrease due to recrystallization with few dislocations within individual grains.
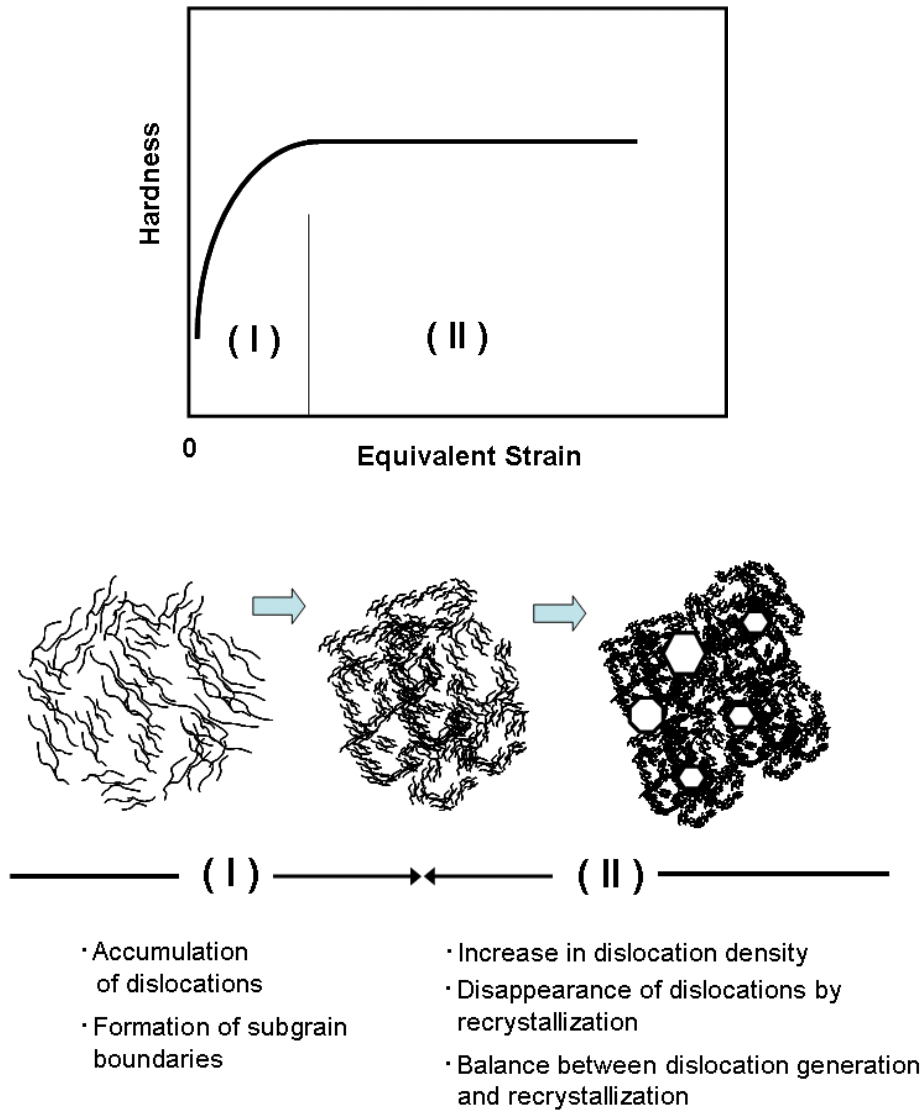
Fig. 10. Schematic illustration of microstructural evolution with straining for grain refinement in pure Cu.

5. Summary and conclusions

(1) All values of Vickers microhardness fall on a unique singe line when plotted as a function of equivalent strain for both disc and ring samples of pure Cu processed by HPT.

(2) The hardness increases with an increase in the equivalent strain at an early stage of straining but levels off and enters into a steady-state where the hardness remains unchanged with further straining.

(3) Tensile properties such as the ultimate tensile strength, uniform elongation and elongation to failure are also expressed by the single function with the equivalent strain.

(4) A subgrain structure develops at an early stage of straining with individual grains containing dislocations. The subgrain size is decreased while the misorientation angle is increased and more dislocations are formed within the grains with further straining. In the steady-state region, some recrystallized grains appear which are free from dislocations.

(5) The difference in dislocation mobility such as stacking fault energy and straining temperature

11

introduces the difference in the hardness variation and microstructural evolution with respect to equivalent strain.

(6) The grain refinement may be achieved by the dislocation coalescence at an early stage of straining but at the later stage the recrystallization is involved where the dislocation accumulation reaches a critical level.

Acknowledgements

References

[1]   R.Z. Valiev, R.K. Islamgaliev, I.V. Alexandrov, Prog. Mater. Sci. 45 (2000) 103–189.

[2]   R.Z. Valiev, T.G. Langdon, Prog. Mater. Sci. 51 (2006) 881–981.

[3]   R.Z. Valiev, Y. Estrin, Z. Horita, T.G. Langdon, M.J. Zehetbauer, Y.T. Zhu, JOM 58 (4) (2006) 33–39.

[4]   N.A. Smirnova, V.I. Levit, V.I. Pilyugin, R.I. Kuznetsov, L.S. Davydova, V.A. Sazonova, Fiz. Met. Metalloved. 68 (1986) 1170–1177.

[5]   T. Hebesberger, H.P. Stuwe, A. Vorhauer, F. Wetscher, R. Pippan, Acta Mater. 53 (2005) 393–402.

[6]   Z. Horita, D.J. Smith, M. Furukawa,M.Nemoto, R.Z. Valiev, T.G. Langdon, J. Mater. Res. 11 (1996) 1880–1890.

[7]   V. Stolyarov, R.Z. Valiev, in: M.J. Zehetbauer, R.Z. Valiev (Eds.), Nanomaterials by Severe Plastic Deformation, Wiley–VCH,Weinheim, Germany, 2004, pp. 125–130.

[8]   C.Rentenberger, T.Waitz, H.P. Karnthaler,Mater. Sci. Eng.A462 (2007) 283–288.

[9]   B.W. Bridgman, Studies in Large Plastic Flowand Fracture, 1st ed., McGraw-Hill, New York, NY, 1952.

[10]   S. Erbel, Met. Technol. 6 (1979) 482–486.

[11]   I. Saunders, J. Nutting, Met. Sci. 18 (1984) 571–575.

[12]   Y. Harai, Y. Ito, Z. Horita, Scripta Mater. 58 (2008) 469–472.

[13]   A.P. Zhilyaev, S. Lee, G.V. Nurislamova, R.Z. Valiev, T.G. Langdon, Scripta Mater. 44 (2001) 2753–2758.

[14]   A.P. Zhilyaev, G.V. Nurislamova, B.K. Kim,M.D. Baro, J.A. Szpunar, T.G. Langdon, Acta Mater. 51 (2003) 753–765.

[15]   F.Wetscher, A. Vorhauer, R. Stock, R. Pippan, Mater. Sci. Eng. A 387–389 (2004) 809–816.

[16]   A. Vorhauer, R. Pippan, Scripta Mater. 51 (2004) 921–925.

[17]   G. Sakai, Z. Horita, T.G. Langdon, Mater. Sci. Eng. A 393 (2005) 344–351.

[18]   C. Xu, Z. Horita, T.G. Langdon, Acta Mater. 55 (2007) 203.

[19]   Y. Ito, Z. Horita, Mater. Sci. Eng. A, doi:10.1016/j.msea.2008.03.055, in press.

[20]   J.P. Hirth, J. Lothe, Theory of Dislocations, 2nd ed., McGraw-Hill, New York, NY, 1968.

[21]   H. Mehrer, Numerical data and functional relationships in science and technology, in: Diffusion in Solid Metals and Alloys, vol. 26, Springer-Verleg, Berlin, 1990.

[22]   P.G. Shewmon, Diffision in Solids, 1st ed., McGraw-Hill, New York, NY, 1963.